Reconfigurable Cavity Bandpass Filters Using Fluid Dielectric

Rui-Sen Chen, *Student Member, IEEE*, Sai-Wai Wong, *Senior Member, IEEE*, Jing-Yu Lin, *Student Member, IEEE*, Yang Yang, *Senior Member, IEEE*, Yin Li, *Member, IEEE*, Long Zhang, *Member, IEEE*, Yejun He, *Senior Member, IEEE*, and Lei Zhu, *Fellow, IEEE*

***Abstract*—A novel method for the development of a reconfigurable cavity bandpass filter using fluid dielectric is proposed. Dielectric material can produce an effective permittivity $\varepsilon_{\mathrm{eff}}$ of the resonant mode when it is loaded into the cavity. Thus, a tube filled with fluid dielectric, e.g., distilled water, can achieve controlled and reversible $\varepsilon_{\mathrm{eff}}$ by adjusting the amount of water in the tube. The same manner of resonant frequency can be achieved as the resonant frequency is related to $\varepsilon_{\mathrm{eff}}$, and then frequency tuning is realized. The fluid property can realize easier and faster tuning mechanism than conventional solid dielectric. As $\varepsilon_{\mathrm{eff}}$ is affected by the loaded dielectric parallel to the electric field, a triple-mode resonator with resonant modes TE_{101}, TE_{011}, and TM_{110}, which have orthogonal electric fields, is investigated to realize tri-band reconfiguration. The $\varepsilon_{\mathrm{eff}}$, as well as the resonant frequencies, corresponding to each mode can be individually controlled by adjusting their related water posts. Then, reconfigurable single-band and tri-band bandpass filters are designed. A reconfigurable tri-band cavity filter using a triple-mode cavity resonator and fluid dielectric with individual and continuous frequency tuning is reported for the first time. Finally, the reconfigurable tri-band filter is fabricated and measured to validate the concept.**

***Index Terms*—Bandpass filters, distilled water, fluid dielectric, metal cavity, reconfigurable cavity filter, triple-mode resonator (TMR).**

Manuscript received January 21, 2020; revised April 20, 2020 and June 11, 2020; accepted July 8, 2020. Date of publication July 21, 2020; date of current version June 16, 2021. This work was supported in part by the Shenzhen Science and Technology Programs under Grant JCYJ20180305124543176 and Grant JCYJ 20190728151457763, in part by the Natural Science Foundation of Guangdong Province under Grant 2018A030313481, and in part by the Shenzhen University Research Startup Project of New Staff under Grant 860-000002110311. *(Corresponding author: Sai-Wai Wong.)*

Rui-Sen Chen is with the College of Electronics and Information Engineering, Shenzhen University, Shenzhen 518060, China, and also with the Department of Electrical and Computer Engineering, Faculty of Science and Technology, University of Macau, 999078, Macau (e-mail: crs13763378709@163.com).

Sai-Wai Wong, Yin Li, Long Zhang, and Yejun He are with the College of Electronics and Information Engineering, Shenzhen University, Shenzhen 518060, China (e-mail: wongsaiwai@ieee.org; liyinuestc@gmail.com; long.zhang@szu.edu.cn; heyejun@126.com).

Jing-Yu Lin and Yang Yang are with the School of Electrical and Data Engineering, University of Technology Sydney, Ultimo NSW 2007, Australia (e-mail: l.j.2014@ieee.org; yang.yang.au@ieee.org).

Lei Zhu is with the Department of Electrical and Computer Engineering, Faculty of Science and Technology, University of Macau, 999078, Macau (e-mail: leizhu@umac.mo).

Color versions of one or more of the figures in this article are available online at http://ieeexplore.ieee.org.

Digital Object Identifier 10.1109/TIE.2020.3009566

I. Introduction

RECONFIGURABLE devices are highly demanded for modern communication systems with varying frequencies and multiband operations. Reconfigurable filters are among the key components for emerging wideband and multifunctional RF front-ends. The most reported reconfigurable filters are implemented on the planar circuits using the varactor-tuned resonators [1]–[7], as the varactors are easily integrated on the planar circuits. Recently, novel reconfigurable planar filters based on microfluidical tuning are reported in [8]–[12]. In [8]–[10], the fluid water is used to modify the relative permittivity of substrate below the planar transmission line, leading to a shift of the resonant frequency. In [11] and [12], liquid metal is utilized to design tunable planar filters by introducing controlled capacitive loading.

Compared to planar filters, metal cavity filters have a relatively large size, but high unloaded Q-factor and high breakdown voltage, thus, cavity filter are highly demanded in communication systems requiring high power capacity, high selectivity, and low power loss. Reconfigurable cavity filters using metal plungers have been reported in recent literatures [13]–[17], which can adjust the resonators' size and consequently adjust the center frequency. To reduce the power loss caused by the poor mechanical and electrical contacts, a contactless tunable cavity filter is reported in [18]. Another reconfiguration technique is used metal screws/posts to adjust the loaded capacitance of the cavity resonator and then to tune the center frequency [19], [20]. Microfluidically reconfigurable cavity filters based on liquid-actuated metal post [21], [22] are proposed to achieve more flexible frequency tuning than the nonfluid technique proposed in [13]–[20]. The electrically tuned filters, such as using piezoelectric actuator [23] and MEMS [24], can achieve fast tuning mechanism. However, they usually suffer from sensitive fabrication and assembly, which reduce their power handling capacity, as discussed in [21].

Most reported works focused on single-band filters, and few practical realizations of reconfigurable multiband filters have been reported. In [4] and [25], varactor-tuned dualband

0278-0046 © 2020 IEEE. Personal use is permitted, but republication/redistribution requires IEEE permission.
See https://www.ieee.org/publications/rights/index.html for more information.

Authorized licensed use limited to: SHENZHEN UNIVERSITY. Downloaded on December 12,2021 at 03:54:15 UTC from IEEE Xplore. Restrictions apply.

microstrip (MS) filters were designed. In [26] and [27], reconfigurable dualband substrate integrated waveguide (SIW) cavity filters using varactor and piezoelectric actuator were proposed, respectively. In general, the reconfigurable multiband filters were rarely reported with more than two passbands. In [28] and [29], tunable tri-band and quad-band filters using varactors were shown. In these works, each band occupied an independent structure to achieve the individual tuning. Besides, reconfigurable multiband metal cavity filters are difficult to be realized. In [20], three groups of coaxial resonators with tuning metal screws were used to design a tunable tri-band filter. However, until now, no fluidly reconfigurable multiband metal cavity filter up to three bands using a multimode cavity resonator has been reported in open literatures.

In this article, a novel reconfiguration technique for cavity filter using fluid dielectric is proposed. The cavity mode is perturbed by the fluid dielectric, which can produce a varying effective permittivity and realize the frequency tuning. The distilled water is chosen as the loaded dielectric for its high permittivity and low cost. Besides, the fluid property of the distilled water can achieve easier, faster, and more flexible tuning mechanism than the solid dielectric post, as the distilled water can be easily controlled by injecting or removing the water in the tubes using the electrical-controlled micropump. The triple-mode resonator (TMR) with resonant modes TE_{101}, TE_{011}, and TM_{110} is then used to realize tri-band reconfiguration. The resonant modes are only affected by the water post (WP) parallel to their own electric fields. Thus, each mode can be individually tuned by adjusting their corresponding WPs without the effect on other resonant modes. The proposed approach shows high feasibility in the design of reconfigurable cavity filters. A single-band and tri-band filters based on single-mode and triple-mode cavity resonators are presented. The measurement of a second-order tri-band filter verifies the design concept. Furthermore, a fully reconfigurable tri-band filter is presented. Additional WPs are employed to control the external couplings and interresonator couplings of the three passbands, which can enhance the tuning range and can also achieve constant bandwidths during the frequency tuning.

II. Fluid-Dielectric Reconfiguration Technique for Cavity Resonator

A. Basic Principal of Cavity Resonator Using Fluid Dielectric

The configuration of the proposed frequency-tuning cavity resonator is plotted in Fig. 1(a) with marked dimensions. The horizontal slot is used to excite the TE_{101} mode, whose long side is perpendicular to the electric field of the TE_{101} mode (E_y), and the resonant frequency is calculated as follow:

$$f(TE_{101}) = \frac{v}{2\sqrt{\varepsilon_{\mathrm{eff}}}}\sqrt{\left(\frac{1}{a}\right)^2 + \left(\frac{1}{c}\right)^2} \quad (1)$$

where v is the light speed in the air, $\varepsilon_{\mathrm{eff}}$ is the effective permittivity corresponding to the TE_{101} mode, a and c are the side lengths of the metal cavity. According to the abovementioned equation,

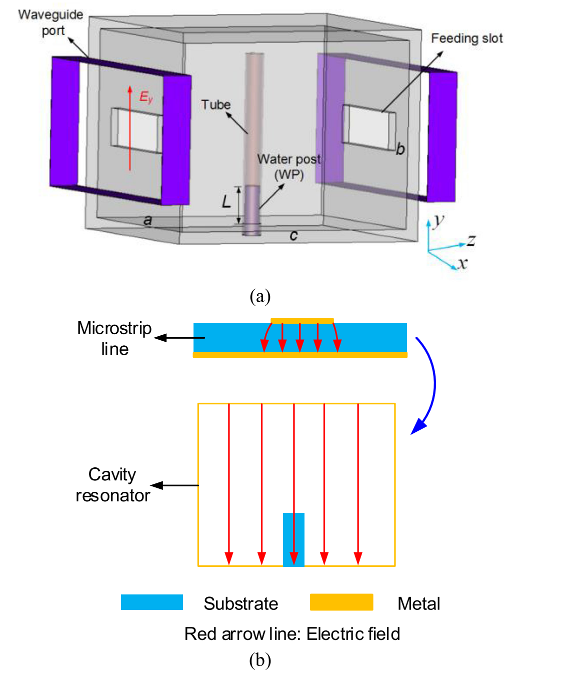

Fig. 1. (a) Three-dimensional view of proposed frequency-tuning cavity resonator with $a = 45$ mm, $b = 50$ mm, $c = 50$ mm. (b) Planar and cavity structures with loaded substrate.

the tunable frequency can be achieved in the following two main approaches:

1) adjust a or c, i.e., the size of the resonator, which can be referred to [13]–[17];
2) adjust effective dielectric permittivity $\varepsilon_{\mathrm{eff}}$.

The planar structures, such as a MS line, the dielectric substrate below the MS line affects the electric field, and then introduce the frequency shift, this inspires us to place a substrate inside the cavity with the direction along the electric field of the resonant mode, as show in Fig. 1(b), which can also introduce the frequency shift. Thus, a tube along y-direction filled with distilled water is put at the center of XZ-plane, as shown in Fig. 1(a). All the waveguide ports used in this article are WR284 standard waveguides.

$$\Delta f_{L,L+d} = f_L - f_{L+d} = \left(\frac{\sqrt{\varepsilon_{\mathrm{eff}}^{L+d}} - \sqrt{\varepsilon_{\mathrm{eff}}^{L}}}{\sqrt{\varepsilon_{\mathrm{eff}}^{L+d}}\cdot\sqrt{\varepsilon_{\mathrm{eff}}^{L}}}\right) \cdot \frac{v}{2}\sqrt{\left(\frac{1}{a}\right)^2 + \left(\frac{1}{c}\right)^2}$$
$$= \left(\frac{\Delta\varepsilon_{\mathrm{eff}}^{L+d}}{(\varepsilon_{\mathrm{eff}}^{L} + \Delta\varepsilon_{\mathrm{eff}}^{L+d})\sqrt{\varepsilon_{\mathrm{eff}}^{L}} + \varepsilon_{\mathrm{eff}}^{L}\sqrt{\varepsilon_{\mathrm{eff}}^{L} + \Delta\varepsilon_{\mathrm{eff}}^{L+d}}}\right) \cdot \frac{v}{2}\sqrt{\left(\frac{1}{a}\right)^2 + \left(\frac{1}{c}\right)^2} \quad (2)$$

$$\Delta\varepsilon_{\mathrm{eff}}^{L,L+d} = F(L, d, \varepsilon_r, r). \quad (3)$$

Authorized licensed use limited to: SHENZHEN UNIVERSITY. Downloaded on December 12,2021 at 03:54:15 UTC from IEEE Xplore. Restrictions apply.

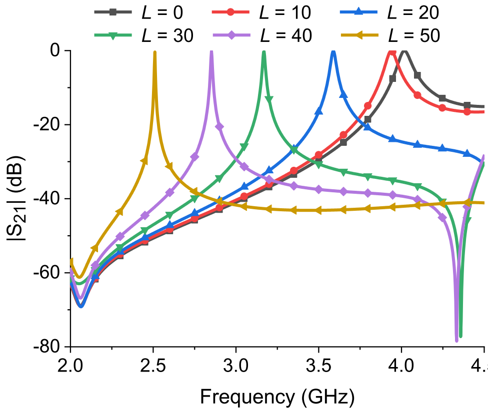

Fig. 2. Simulated $|S_{21}|$ with different length of loaded WP.

Equation (2) gives the frequency variation produced by the varied length of WP, where $\Delta f_{L,L+d}$ and $\Delta\varepsilon_{\text{eff}}^{L,L+d}$, respectively, represent the variations of frequency and effective permittivity when the post length is increased from L to $L+d$, while f_L, f_{L+d}, $\varepsilon_{\text{eff}}^{L}$, and $\varepsilon_{\text{eff}}^{L+d}$ represent the resonant frequencies and effective permittivity corresponding to the post length L and $L+d$, respectively. d is the increment of post length. The varied effective permittivity is depended on different perturbations on the cavity mode TE_{101}. The perturbation is produced by the loaded water. Thus, the $\Delta\varepsilon_{\text{eff}}^{L,L+d}$ is a function of L, d, ε_r, and r, as given in (3), which is the intrinsic factor that produces the frequency tuning. According to (2), a large $\Delta\varepsilon_{\text{eff}}^{L,L+d}$ can produce a large $\Delta f_{L,L+d}$. As the electric field is not uniformly distributed in the cavity, especially under the perturbation of the WP, same increment of WP in different starting length will cause different perturbation on the cavity mode, and then produce different $\Delta\varepsilon_{\text{eff}}^{L,L+d}$ as well as the $\Delta f_{L,L+d}$, which can be expressed as the following equations. Besides, it is easy to obtain that for a same starting post length L, a larger increment d can produce a larger frequency shift.

$$\Delta\varepsilon_{\text{eff}}^{L,L+d} \neq \Delta\varepsilon_{\text{eff}}^{L+s,L+s+d} \tag{4}$$

$$\Delta f_{L+d,L} \neq \Delta f_{L+s+d,L+s}. \tag{5}$$

B. Frequency Tuning

The frequency tuning produced by the varied WP is then presented. Fig. 2 shows the simulated $|S_{21}|$ with respect to the length of WP, which can give a direct insight into the frequency tuning of the proposed design concept. We see that the resonant frequency of the filter shifts to the lower frequency when increasing the length of WP, which is due to that longer WP produces increasing perturbation on the mode, and enlarges the varied effective permittivity $\Delta\varepsilon_{\text{eff}}^{L,L+d}$ and then produces a larger frequency shift. Besides, it can be also seen that the same increment of post length $d = 10$ mm at different initial length of the WP produce different frequency shifts, e.g., $\Delta f_{0,10}$ is about 80 MHz, while $\Delta f_{20,30}$ is about 420 MHz, as analyzed in (4) and (5). This indicates that the frequency shift produced by the loaded dielectric post is not a simple function of the dielectric volume.

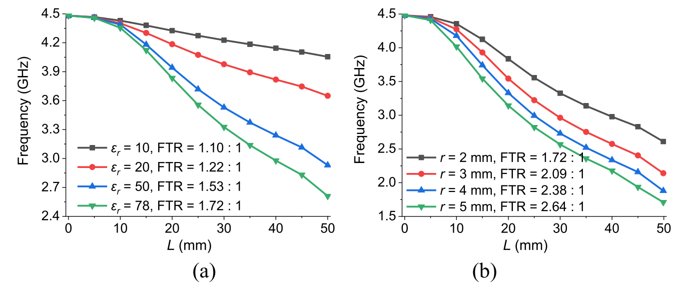

Fig. 3. Comparison of tuning range versus. (a) Different permittivity ε_r. (b) Different radius r.

In a substrate-based planar structure, higher permittivity can obtain lower frequency for the same size of the resonator. Similarly, substrate with lower/higher permittivity applied to Fig. 1(a) will introduce a smaller/larger frequency tuning range. Fig. 3(a) plots the tuning range with different permittivity $\varepsilon_r = 10/20/50/78$. The resonant frequencies here are obtained using the eigenmode solver of CST simulator, which can present an accurate effect of the dielectric post on the resonant frequencies without other loading effects, such as feeding slots (FSs). The frequency tuning ratios (FTRs) with four permittivity are 1.10, 1.22, 1.52, and 1.72, respectively. The FTR is defined as $\text{FTR} = f_{\max}/f_{\min}$, where $f_{\max}$ is the highest center frequency, and $f_{\min}$ is the lowest center frequency within the tuning range. Thus, a higher permittivity can be used to obtain a larger tuning range. The distilled water has high permittivity but low cost and easy access.

Then, the radius of the WP is considered, as shown in Fig. 3(b). It can be seen that the tuning range can be widen by introducing a large post radius. The FTR is increased from 1.72:1 to 2.64:1 when the radius is increased from 2 to 5 mm.

In practical realization of a proposed reconfigurable cavity filter, the length L is used to tune the resonant frequency, as the amount of distilled water can be easily controlled by injecting or removing the water in the tubes using the electrical-controlled micropump, which is superior to a solid dielectric post.

C. Unloaded Q-Factor

The unloaded Q-factor Q_u of a cavity-based resonator is determined by three parts: conductor loss, dielectric loss, and radiation loss. Thus, the Q_u is calculated using the following equation:

$$\frac{1}{Q_u} = \frac{1}{Q_{uc}} + \frac{1}{Q_{ud}} + \frac{1}{Q_{ur}} \tag{6}$$

where Q_{uc} is Q_u only with conductor loss, Q_{ud} is Q_u only with dielectric loss, Q_{ur} is Q_u only with radiation loss. As proposed cavity resonator is a closed structure, the radiation loss is neglected. The metal used for the cavity is lossy copper with electrical conductivity of 5.8e+7 S/m.

Authorized licensed use limited to: SHENZHEN UNIVERSITY. Downloaded on December 12,2021 at 03:54:15 UTC from IEEE Xplore. Restrictions apply.

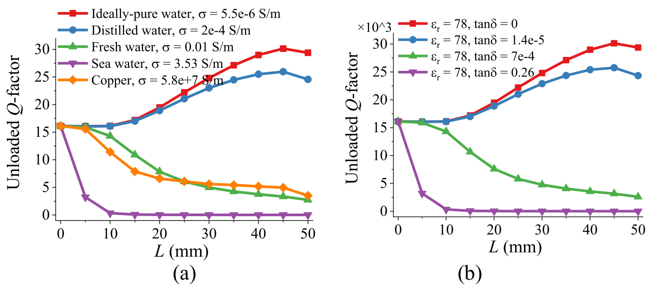

Fig. 4. Unloaded Q-factor. (a) Against different types of water and copper metal post. (b) Against dielectric materials with different loss tangent.

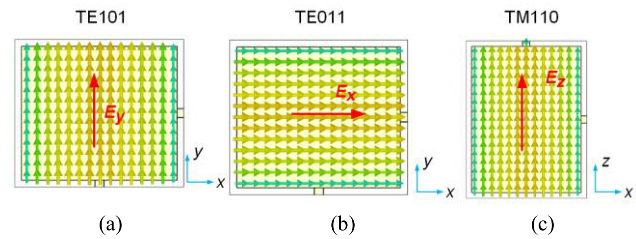

Fig. 5. Electric field distribution of three RWG orthogonal modes. (a) TE_{101} (E_y). (b) TE_{011} (E_x). (c) TM_{110} (E_z).

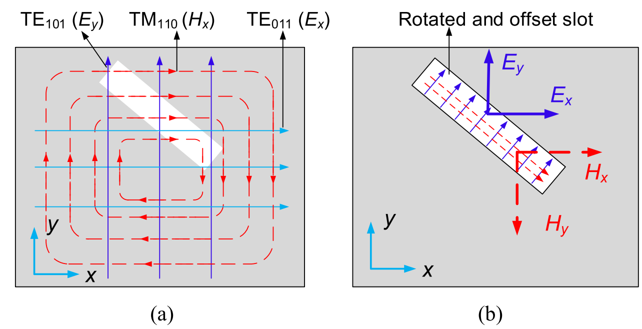

Fig. 6. (a) Electric field distributions of TE_{101}, TE_{011} and magnetic field distribution of TM_{110}. (b) Excitation mechanism. Solid-arrow line: Electric field; Dash-arrow line: Magnetic field.

Fig. 4(a) shows the Q_u of the cavity resonator affected by different types of the water and copper metal post. The water model in the simulator (CST and HFSS) is defined as the dielectric with $\tan\delta = 0$, but with a nonzero electrical conductivity, as given in Fig. 4(a). The increasing length of metal post results in decreasing Q_u due to the increasing conductor loss. Different types of water have different effect on Q_u. The increasing amount of water can enhance the binding effect on the electromagnetic (EM) field and reduce the EM energy dissipating on the conductor walls. However, the nonzero electrical conductivity will produce extra power loss. The ideally pure and distilled water (used in this work) have very small electrical conductivity. Thus, the power loss can be neglected, which consequently improves the Q_u when L increases. As a result, they both have higher Q_u than the copper metal post. The fresh water and sea water have, respectively, electrical conductivity of 0.01 and 3.53 S/m. The power loss of water dominates the Q_u, and the increasing amount of L causes a decreasing Q_u. Thus, the power loss produced by the nonzero electrical conductivity of water can be equivalent to a dielectric with nonzero loss tangent and zero electrical conductivity. Fig. 4(b) shows the Q_u affected by four dielectrics with purposely given loss tangents. It can be seen that each dielectric has same effect on Q_u compared to each type of water, e.g., the distilled water can be as a dielectric with loss tangent 1.4e–5, and the fresh water can be as a dielectric with loss tangent 0.0007. While the seawater has large electrical conductivity and acts as a dielectric with loss tangent up to 0.26, these corresponding relationships are obtained under the particular dimensions of the proposed resonator.

D. Tri-Band Reconfiguration Based on TMR

To achieve a tri-band filter, a triple mode cavity resonator is introduced. The most-used rectangular waveguide (RWG) mode is the TE_{101}, which has a pure y-direction electric field, as shown in Fig. 5(a). In fact, there are two other RWG modes with the pure x-direction and pure z-direction electric field, which are corresponding to TE_{011} and TM_{110} modes, as shown in Fig. 5(b) and (c), respectively. These three modes are isolated to each other due to the orthogonal field distributions. Their resonant frequencies are calculated using the following equations, where each mode is determined by two side's lengths of the cavity:

$$f_1(\mathrm{TE}_{101}) = \frac{v}{2\sqrt{\varepsilon_{\mathrm{eff}}^{I}}}\sqrt{\left(\frac{1}{a}\right)^2 + \left(\frac{1}{c}\right)^2} \tag{7a}$$

$$f_2(\mathrm{TE}_{011}) = \frac{v}{2\sqrt{\varepsilon_{\mathrm{eff}}^{II}}}\sqrt{\left(\frac{1}{b}\right)^2 + \left(\frac{1}{c}\right)^2} \tag{7b}$$

$$f_3(\mathrm{TM}_{110}) = \frac{v}{2\sqrt{\varepsilon_{\mathrm{eff}}^{III}}}\sqrt{\left(\frac{1}{a}\right)^2 + \left(\frac{1}{b}\right)^2} \tag{7c}$$

where v is the light speed in the air, $\varepsilon_{\mathrm{eff}}^{I}$, $\varepsilon_{\mathrm{eff}}^{II}$, and $\varepsilon_{\mathrm{eff}}^{II}$ are the effective permittivity corresponding to TE_{101}, TE_{011}, and TM_{110} modes, respectively, a, b, and c are the side lengths of the metal cavity.

These three modes are inherent property of the RWG resonator; however, to use these modes to design practical components, the excitation method of the three modes is first discussed. Fig. 6(a) shows the electric field distribution of TE_{101}, TE_{011} and the magnetic field distribution of TM_{110} at XY-plane where FS locates. Clearly, the horizontal slot can excite TE_{101} and the rotated slot can excite the TE_{101}, TE_{011} mode by the electric components. These two types of slots cannot excite TM_{110} as the integral of TM_{110}'s magnetic field within the nonoffset slot is zero due to the center-symmetry structures. Thus, an offset slot is needed to excite TM_{110}. As a result, a rotated and offset slot can excite all the three modes, as shown in Fig. 6(b).

Authorized licensed use limited to: SHENZHEN UNIVERSITY. Downloaded on December 12,2021 at 03:54:15 UTC from IEEE Xplore. Restrictions apply.

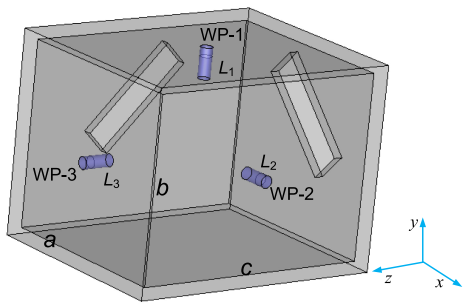

Fig. 7. Proposed tri-band frequency-tuning cavity resonator with $a = 65$ mm, $b = 56$ mm, and $c = 80$ mm.

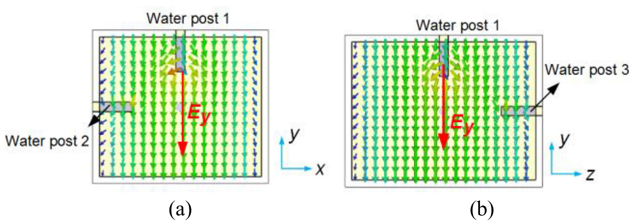

Fig. 8. Effect of the WPs on the electric field distribution of TE_{101} (E_y) mode. (a) Post 1 and post 2. (b) Post 1 and post 3.

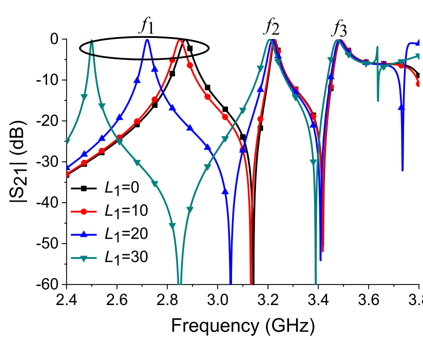

Fig. 9. Frequency-tuning of the TMR against L_1.

The configuration of single-cavity tri-band filter is shown in Fig. 7. The rotated and offset FSs are used to excite these three modes. Three WPs at the centers of three orthogonal metal walls are used to tune the frequency. Then, we first analyzed how the WPs in different positions affect the resonant modes. For instance, the effect of the three WPs on the TE_{101} mode is shown in Fig. 8. It can be seen that only WP 1, which has same direction of TE_{101}'s electric field, perturbs the electric field and produces a varied εI eff to obtain a frequency shift of TE_{101}, which can be referred to (7a). Similarly, WPs 2 and 3 perturb the electric field of TE_{011} and TM_{110} modes and produce varied $\varepsilon_{\text{eff}}^{II}$ and $\varepsilon_{\text{eff}}^{III}$ to obtain frequency shifts of TE_{011} and TM_{110} modes, respectively. Thus, each WP only causes the frequency shift of its corresponding resonant modes whose electric-field's direction is parallel to the WP. Fig. 9 shows the frequency-tuning of the TMR versus varying WPs' lengths L_1. The varying length of WP-1 (L_1) only cause frequency shift of f_1 without effect on f_2 and f_3. Similarly, L_2 and L_3 only affect f_2 and f_3, respectively.

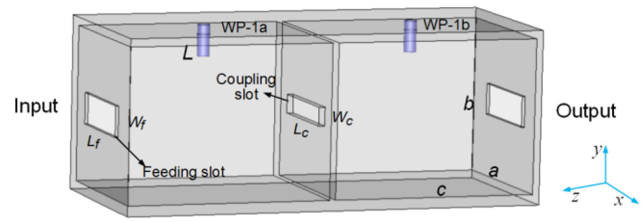

Fig. 10. Configuration of second-order single-band filter using two cavities with same size.

This is an attractive property that all the three resonant modes can be individually tuned by their corresponding WPs without the effect on other resonant modes.

III. Design of Reconfigurable Filters

A. Single-Band Reconfigurable Filter

Then, the proposed reconfiguration technique is used to design reconfigurable bandpass cavity filters. Fig. 10 shows the configuration of a second-order single-band filter using two identical metal cavities. Each cavity produces a TE_{101} mode and couples to each other through the coupling slots (CSs) between the two cavities, and two WPs are placed at the center of the top walls of each cavity.

First, the filter synthesis method is utilized to design the second-order bandpass filter, the external Q-factor and coupling coefficients can be calculated as [30]

$$Q_e = \frac{g_0 g_1}{\text{FBW}}, \; K_{12} = \frac{\text{FBW}}{\sqrt{g_1 g_2}} \tag{8}$$

where g_0, g_1, and g_2 are the low-pass prototype element values of the second-order Butterworth polynomial, which can be set as $g_0 = 1$, $g_1 = g_2 = 1.4142$. With the specifications of 3% fractional bandwidth (FBW), $Q_e = 47$ and $K_{12} = 0.021$ are obtained.

For the practical filter, the Q_e and K are extracted using the following formulas [30]:

$$Q_e = \frac{f_0}{\Delta f_{3-\text{dB}}}, K = \pm \frac{f_{p1}^2 - f_{p2}^2}{f_{p1}^2 + f_{p2}^2} \tag{9}$$

where f_{p1} and f_{p2} are the resonant frequencies of the two coupled resonators, f_0 is the center frequency, and$\Delta f_{3\text{-}dB}$ is bandwidths between +/–90° phase offsetting of the resonant frequency, respectively. For this cavity filter, the Q_e and K_{12} can be controlled by modifying the sizes of FSs and CS, respectively. The optimized result of the bandpass filter is shown in Fig. 11 with $L = 0$, the filter operates at 3.38 GHz with 104 MHz 3-dB bandwidth (BW). The physical dimensions of the proposed single-band filter are given in Table I, the radius of WPs is fixed at 2 mm.

As analyzed in Section II, the frequency tuning is achieved by modifying the amount of water in the tube. Fig. 11 shows the simulated S-parameter with varying WPs' lengths, the tuning range is from 3.95 to 2.73 GHz (1.22 GHz) with the return loss better than 10 dB, and the FTR is 1.45:1, while the insertion loss

Authorized licensed use limited to: SHENZHEN UNIVERSITY. Downloaded on December 12,2021 at 03:54:15 UTC from IEEE Xplore. Restrictions apply.

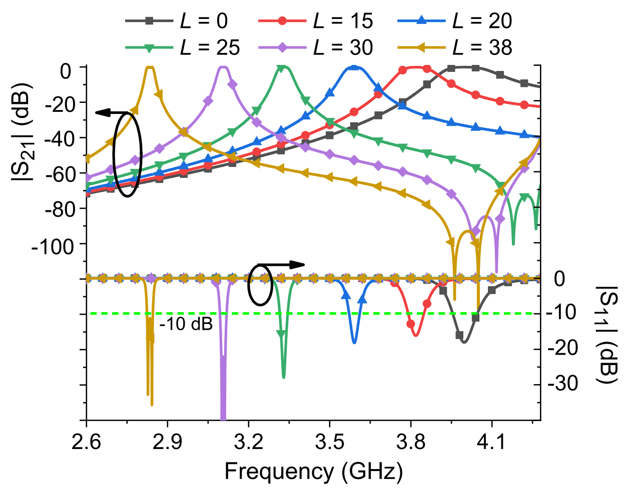

Fig. 11. Simulated results of the second-order single-band filter with varying WPs' lengths.

TABLE I
PHYSICAL DIMENSIONS OF SINGLE-BAND FILTER

Symbol	a	b	c	L_f	W_f	L_c	W_c
Value (mm)	50	50	50	27.5	28	28.5	4

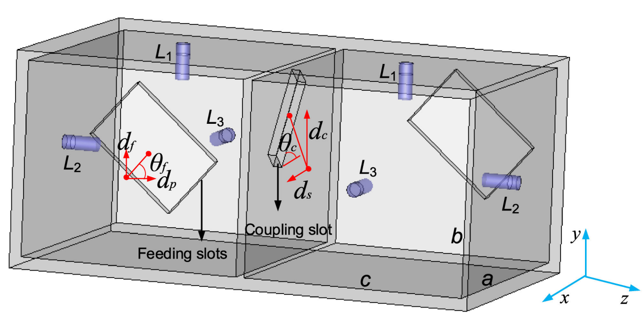

Fig. 12. Configuration of the reconfigurable second-order tri-band filter with two cavity. (Solid dots: Center points of the slots or walls).

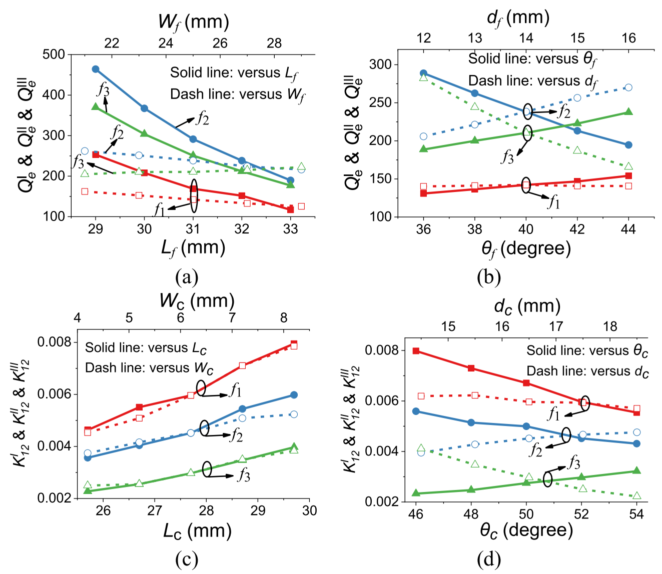

Fig. 13. Variation trend versus physical parameters. (a) and (b) External Q-factors Q_e^{I}, Q_e^{II}, and Q_e^{III}. (c) and (d) Coupling coefficients K_{12}^{I}, K_{12}^{II}, and K_{12}^{III}.

TABLE II
PHYSICAL DIMENSIONS OF TRI-BAND FILTER

a	b	c	L_f	W_f	L_c	W_c
75 mm	55 mm	63 mm	31.1 mm	27.3 mm	27.7 mm	6.4 mm
d_f	d_p	d_c	d_s	θ_f	θ_c	
7.6 mm	6.6 mm	14.3 mm	4.2 mm	40.5°	52°	

has small deterioration from 0.1 to 0.5 dB. The narrowed BW, as plotted in Fig. 11, is due to that the increasing amount of the water enhance the concentration of the EM field around the water and reduces the coupling energy between the two-coupled cavity resonators.

B. Tri-Band Reconfigurable Filter

The last section shows the application of a proposed reconfiguration technique in filter design. Based on that, a tri-band reconfigurable filter is presented. Here, a second-order tri-band reconfigurable filter using two identical cavities is designed, and the configuration is shown in Fig. 12. As analyzed in the last section, the rotated and offset slots can excite the three modes, in the design of the tri-band filter, the feeding and CSs are all rotated and offset. The FSs (length L_f, width W_f) are placed with the rotation angle θ_f, offsetting d_f in y-direction and offsetting d_p in z-direction, and the CS (length L_c, width W_c) is placed with rotation angle θ_c, offsetting d_c in y-direction and offsetting d_s in x-direction. Each cavity has three orthogonal WPs corresponding to the three modes, respectively. The WPs' lengths corresponding to f_1 (E_y), f_2 (E_x), and f_3 (E_z) are L_1, L_2, and L_3, respectively.

Herein, the second-order tri-band filters are synthesized using Butterworth polynomial [30]. With the specifications of 0.9%, 0.7%, and 0.5% for the first, second, and third bands, respectively, the external Q-factors and coupling coefficients are calculated as

$$Q_e^{I} = 157, Q_e^{II} = 202, Q_e^{III} = 282$$
$$K_{12}^{I} = 0.0064, K_{12}^{II} = 0.0049, K_{12}^{III} = 0.0035.$$

The extracted external Q-factors and coupling coefficients versus the physical dimensions are plotted in Fig. 13 using the formula (9). Then, by properly setting the suitable values specified in Fig. 13 to meet the calculated external Q-factors and coupling coefficients, the desired filtering responses are obtained. As shown in Fig. 14(a)–(c) with the condition of $L = 0$, the first band operates at 3.03 GHz with BW 27.2 MHz, the second band operates at 3.32 GHz with BW 22.3 MHz, the third band operates at 3.62 GHz with BW 17.1 MHz, and better than 20 dB RLs are achieved. The physical dimensions are given in Table II, the radius of WPs are fixed at 2 mm.

Authorized licensed use limited to: SHENZHEN UNIVERSITY. Downloaded on December 12,2021 at 03:54:15 UTC from IEEE Xplore. Restrictions apply.

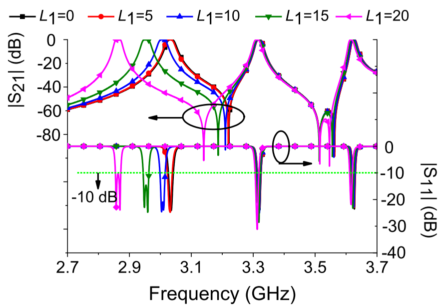

(a)

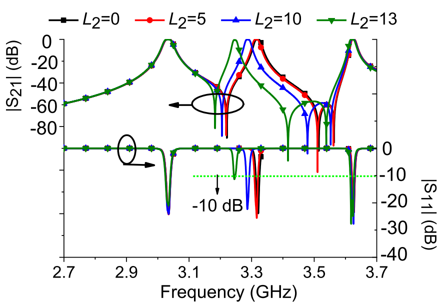

(b)

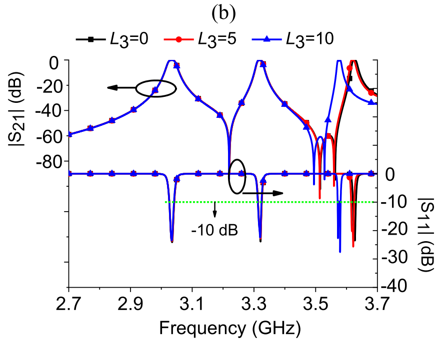

(c)

Fig. 14. Simulated results of the second-order tri-band filter versus different posts' length. (a) L_1. (b) L_2. and (c) L_3.

Fig. 14 also shows the simulated results of the tri-band filter with different length of WPs. Fig. 14(a) indicates that the variation of L_1 only causes the frequency shift of band 1, while it has little effect on band 2 and band 3, which is a distinguished feature of this design. Fig. 14(b) and (c) is similar to the analysis of Fig. 14(a). ILs increase slightly from 0.1 to 0.5 dB, and the FBWs become narrow due to the increasing binding effect of WP. The tuning percentages and tuning ranges of the three bands are 5.9% (169 MHz), 2.5% (80 MHz), and 1.7% (60 MHz) with return loss better than 10 dB, respectively, where the tuning percentage is defined as

$$\eta = \frac{f_{\max} - f_{\min}}{f_{\min}} \times 100\%. \quad (10)$$

IV. Experimental Results

To validate the concept, the proposed reconfigurable tri-band filter is fabricated and measured. Fig. 15 shows the photographs of the fabricated tri-band filter and the actuation mechanism. The filter is measured and tuned by adjusting the amount of distilled water in the tubes; the water level inside the tube can be adjusted by injecting or removing the water via the electrical-controlled micropump. The water can stick to the tubes by itself via the tension and atmospheric pressure due to its small density and gravity. The measured results are shown in Fig. 16(a)–(c) for bands 1–3, respectively. We see that each channel can be

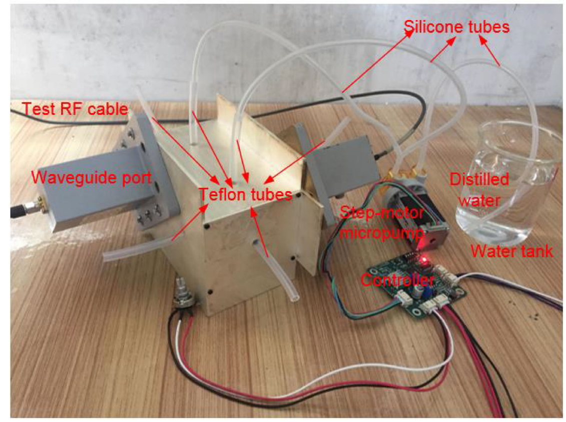

Fig. 15. Actuation mechanism of the proposed filter.

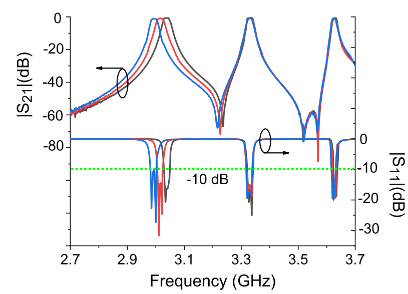

(a)

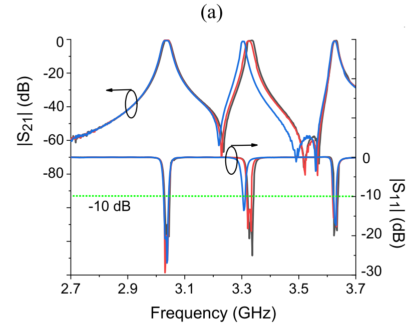

(b)

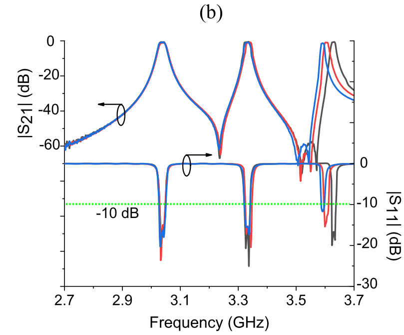

(c)

Fig. 16. Measured results. (a) Frequency tuning of band 1. (b) Frequency tuning of band 2. (c) Frequency tuning of band 3.

Authorized licensed use limited to: SHENZHEN UNIVERSITY. Downloaded on December 12,2021 at 03:54:15 UTC from IEEE Xplore. Restrictions apply.

TABLE III
MEASURED RESULTS OF RECONFIGURABLE TRI-BAND FILTER

	Band 1	Band 2	Band 3
f_{max}/f_{min} (GHz)	3.035/2.986	3.335/3.3	3.632/3.588
TR (MHz)	50	35	44
η	2.3%	1.1%	1.2%
IL (dB)	0.7/1.1	0.75/1.1	0.75/1.15
FBW	0.95%/0.85%	0.71%/0.46%	0.5%/0.38%

Note: $f_{\max}/f_{\min}$: highest/lowest frequency; TR: tuning range; η: tuning percentage; IL: insertion loss; FBW: fractional bandwidth.

individually tuned with little effect on other two bands. As the amount of water can be tuned continuously, the individual and continuous reconfiguration of the proposed tri-band filter can be obtained. The measured results are concluded in Table III. There are some discrepancies between the simulated and measured results due to the fabrication tolerance and roughness of metal surface. In general, the two results both show that the proposed concept has feasibility in the design of reconfigurable multiband cavity filters.

The tunable filter is measured at a static state of water, but allows a varying amount of water to achieve frequency tuning. The flowing water means a fixed amount of water and is not suitable for achieving the frequency tuning. Besides, a slow velocity and a small pressure are more suitable for injecting small and precise amount of the water to achieve the continuous and precise frequency tuning.

V. FULLY RECONFIGURABLE TRI-BAND FILTER

The simulated and measured prototype of the reconfigurable tri-band filter using the distilled water verifies the proposed design concept. As the external couplings and interresonator couplings cannot be tuned when tuning the operating frequencies, which cause the narrowed BW and narrowed tuning range. To tackle these issues and further show the feasibility of the proposed reconfiguration technique, a fully reconfigurable tri-band filter with all the controlling of operating frequencies, external couplings, and interresonator coupling is designed.

The physical structure of the filter is shown in Fig. 17. The conventional standard waveguide port is replaced by the coaxial-to-waveguide transition composed of a feeding cavity, a FS and a probe, as shown in Fig. 17(a). The single CS is replaced by three CSs, i.e., CS-1, CS-2, and CS-3, as shown in Fig. 17(b). These three CSs are the independent coupling structures related to band 1, band 2, and band 3, respectively, which can be referred to Fig. 6. The CS-1 only produce the coupling of the mode with electric filed E_y, the CS-2 only produce the coupling of the mode with electric filed E_z (or magnitude field H_x), while the CS-3 only produce the coupling of the mode with electric filed E_x. Three coupling water posts (CWPs) placed together with the CSs are used to achieve the individually tuned interresonator couplings of the three bands. Two feeding water posts (FWPs) close to the probes are used to obtain tuned external couplings. Three pairs of frequency-tuning water posts (FTWPs) at the center of the cavity wall are used to achieve the frequency tuning.

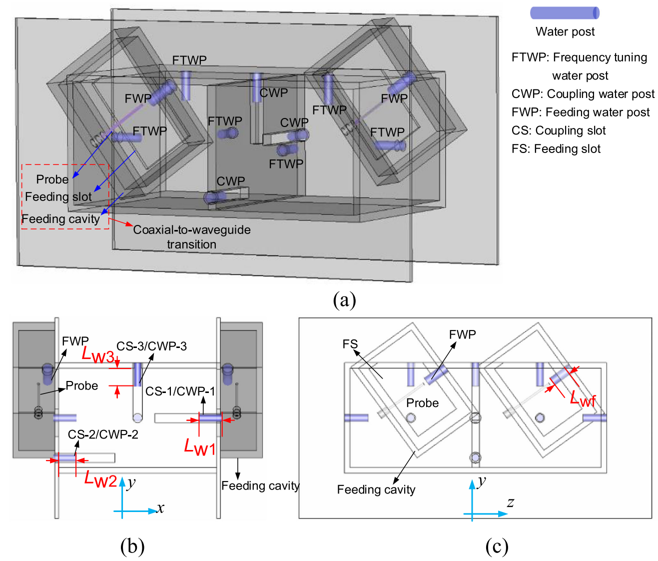

Fig. 17. Physical structure of the fully reconfigurable tri-band filter. (a) Perspective view. (b) Side view in *XY*-plane. (c) Side view in *YZ*-plane.

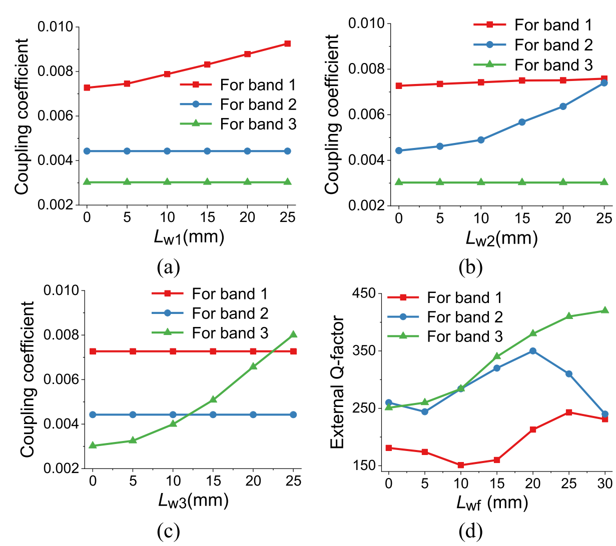

Fig. 18. Effect of the lengths on the CWPs and FWPs. (a) Coupling coefficients versus length of CWP-1. (b) Coupling coefficients versus length of CWP-2. (c) Coupling coefficients versus length of CWP-3. (d) External *Q*-factors versus length of FWP.

Fig. 18 shows the effect of the lengths of the CWPs and FWPs on the coupling coefficients and external *Q*-factors. It can be seen that the enlarged CWPs corresponding to each band can enhance the interresonator coupling, as the CWP can concentrate the EM field around the CS and enhance the coupling energy between the resonators. Besides, each CWP only has effect on its related band. These results also indicate that the coupling of each band can be individually controlled by its related CS and CWP. While the enlarged FWPs will simultaneously affect the external couplings of the three bands, but different effects on

Authorized licensed use limited to: SHENZHEN UNIVERSITY. Downloaded on December 12,2021 at 03:54:15 UTC from IEEE Xplore. Restrictions apply.

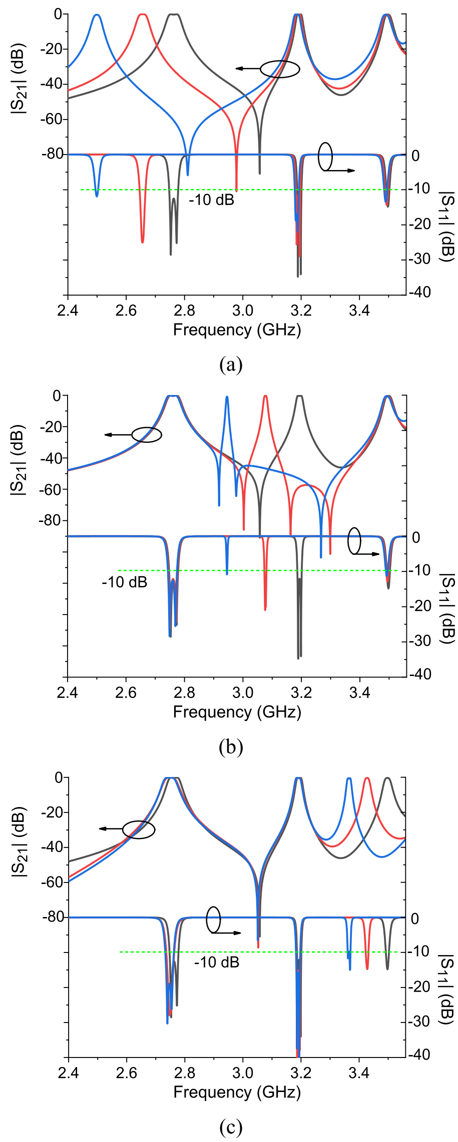

Fig. 19. Simulated results of filter in Fig. 17. (a) Frequency tuning of band 1. (b) Frequency tuning of band 2. (c) Frequency tuning of band 3.

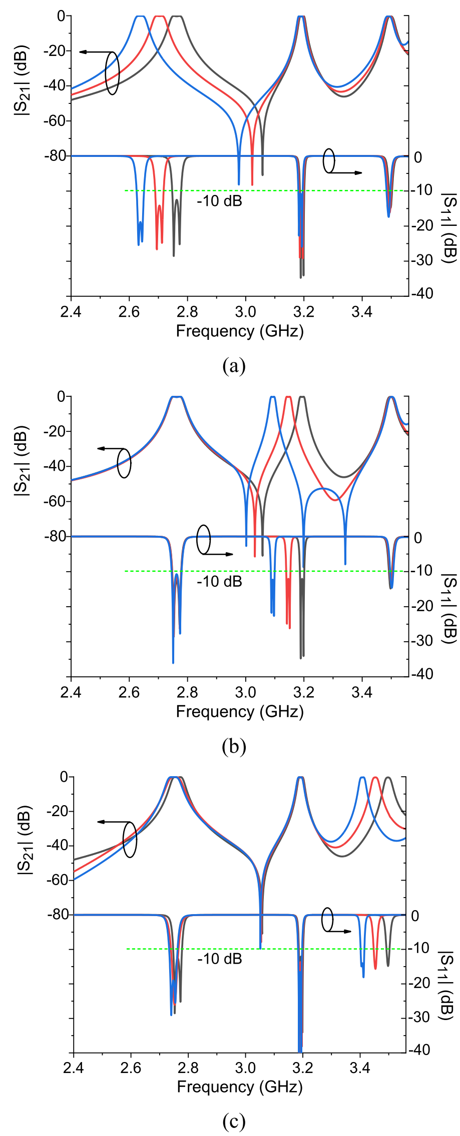

Fig. 20. Simulated results with constant bandwidth. (a) Frequency tuning of band 1. (b) Frequency tuning of band 2. (c) Frequency tuning of band 3.

the three bands, which can still help to tune the in-band filtering performance when tuning the frequency and bandwidth. The enlarged FTWP cause a decreasing resonant frequency, and will also narrow the bandwidths, as analyzed previously.

Then, an enhanced-tuning-range tri-band filter is designed and optimized. The simulated results are shown in Fig. 19. It can be seen that each band can be individually tuned with little effect on other two bands. Compared to the tri-band filter in Fig. 12, the tuning ranges of the three bands are increased to 10.7%, 8.6%, and 4.0%, respectively.

Furthermore, as the interresonator couplings can be individually tuned, constant bandwidths of the three bands can be realized when tuning the frequencies. The narrowed BW caused by the enlarged FTWPs when tuning the frequency can be complemented by enlarging the CWPs. The simulated results for constant bandwidths are shown in Fig. 20.

The bandwidths of the three bands can be kept constant by properly modifying the CWPs and FWPs. The simulated results shown in Figs. 19 and 20 are obtained based on the same filter with same original dimensions except the dimensions of WPs. The comparison of tunable tri-band filters shown in Figs. 12 and 17 is provided in Table IV. The filter shown in Fig. 17 has a wider tuning range and can achieve a constant BW during the frequency tuning.

The comparison with other tunable filters is provided in Table V. The proposed design concept shows the merits of high unloaded *Q*-factor, multiband application, multiband filter in a single multimode resonator, individual and continuous tuning, tunable BW, and electrical control.

Authorized licensed use limited to: SHENZHEN UNIVERSITY. Downloaded on December 12,2021 at 03:54:15 UTC from IEEE Xplore. Restrictions apply.

TABLE IV
COMPARISON OF THE TUNING RANGES OF TWO TRI-BAND FILTERS

Works	Tuning conditions	Tuning range/tuning percentage		
		Band 1	Band 2	Band 3
Fig.12	Measured Varied FBW	50MHz/2.3%	35MHz/1.1%	44MHz/1.2%
	Simulated Varied FBW	169MHz/5.9%	80MHz/2.5%	60MHz/1.7%
Fig.17	Simulated Varied FBW	267MHz/10.7%	252MHz/8.6%	135MHz/4.0%
	Simulated Constant FBW	128MHz/4.9%	102MHz/3.3%	93MHz/2.7%

TABLE V
COMPARISONS WITH REPORTED TUNABLE FILTERS

Ref.	Band No.	Structure	Reso. No.	Tune Type	Tune Tech.	Elec. Tune	Indi. Tune	Cons. BW	Q_u
[4]	2	MS	2	Disc.	Varactor	Yes	Yes	No	Low
[11]	1	CPW	1	Disc.	Liquid Metal	No.	N.A.	No	Low
[20]	3	Coaxial cavity	3	Cont.	Metal Screw	No	Yes	No	High
[21]	1	Coaxial cavity	1	Cont.	Liquid Metal	Yes	N.A.	Yes	Middle
[23]	1	Coaxial cavity	1	Cont.	Piezo actuator	Yes	N.A.	Yes	Middle
[29]	4	MS	4	Cont.	Varactor	Yes	Yes	Yes	Low
T.W. Fig.12	3	RWG	1	Cont.	Fluid Dielectric	Yes	Yes	No	High
T.W. Fig.17	3	RWG	1	Cont.	Fluid Dielectric	Yes	Yes	Yes	High

Band No.: Number of passbands; Reso. No.: Number of resonators for the multiband; Filter structure; Tune Tech.: Tune technique; Elec. Tune: Electrical tune; Indi. Tune: Individual tune; Cons. BW: Constant bandwidth; Q_u; Unloaded Q-factor; MS: MS line; CPW; Coplanar waveguide; RWG: Rectangular waveguide; Disc.: Discrete; Cont.: Continuous; N.A.: Not applicable; T.W.: This work.

VI. CONCLUSION

In this article, a novel reconfiguration technique for cavity components based on fluid dielectric was proposed. The loaded fluid dielectric, i.e., distilled water, produced an effective permittivity corresponding to the cavity mode, and then realized the frequency tuning. Then, a TMR with orthogonal electric field distributions was investigated to achieve the tri-band reconfigurable filter with individual frequency tuning. The distilled water allowed an easy, fast, and flexible tuning mechanism by controlling the micropump to inject or remove accurate amount of water in the tubes. High permittivity and low dielectric loss brought in large tuning range and low insertion loss. Reconfigurable single-band and tri-band filters were then designed, and the measurement of the tri-band filter verified the design concept. A fully reconfigurable tri-band filter was finally presented to show that the fluid dielectric had high feasibility and attractive feature in designing reconfigurable cavity filters.

REFERENCES

[1] J. Xu and Y. Zhu, “Tunable bandpass filter using a switched unable diplexer technique,” *IEEE Trans. Ind. Electron.*, vol. 64, no. 4, pp. 3118–3126, Apr. 2017.

[2] X. Y. Zhang, C. H. Chan, Q. Xue, and B.-J. Hu, “RF tunable bandstop filters with constant bandwidth based on a doublet configuration,” *IEEE Trans. Ind. Electron.*, vol. 59, no. 2, pp. 1257–1265, Feb. 2012.

[3] J.-X. Chen, Y. Ma, J. Cai, L.-H. Zhou, Z.-H. Bao, and W. Che, “Novel frequency-agile bandpass filter with wide tuning range and spurious suppression,” *IEEE Trans. Ind. Electron.*, vol. 62, no. 10, pp. 6428–6435, Oct. 2015.

[4] C.-F. Chen, “A compact reconfigurable microstrip dual-band filter using varactor-tuned stub-loaded stepped-impedance resonators,” *IEEE Microw. Wireless Compon. Lett.*, vol. 23, no. 1, pp. 16–18, Jan. 2013.

[5] Z. Wang, J. R. Kelly, P. S. Hall, A. L. Borja, and P. Gardner, “Reconfigurable parallel coupled band notch resonator with wide tuning range,” *IEEE Trans. Ind. Electron.*, vol. 61, no. 11, pp. 6316–6326, Nov. 2014.

[6] J.-X. Chen, Y.-J. Zhang, J. Cai, Y.-L. Li, and Y.-J. Yang, “Overall study of frequency-agile mechanism of varactor-loaded λ/4 resonator for designing tunable filter with stable wide stopband,” *IEEE Trans. Ind. Electron.*, vol. 66, no. 8, pp. 6302–6310, Aug. 2019.

[7] H. Guo, J. Ni, and J. Hong, “Varactor-tuned dual-mode bandpass filter with nonuniform *Q* distribution,” *IEEE Microw. Wireless Compon. Lett.*, vol. 28, no. 11, pp. 1002–1004, Nov. 2018.

[8] D. L. Diedhiou, R. Sauleau, and A. V. Boriskin, “Microfluidically tunable microstrip filters,” *IEEE Trans. Microw. Theory Techn.*, vol. 63, no. 7, pp. 2245–2252, Jul. 2015.

[9] W.-J. Zhou and J.-X. Chen, “Novel microfluidically tunable bandpass filter with precisely-controlled passband frequency,” *Electron. Lett.*, vol. 52, no. 14, pp. 1235–1236, Jul. 2016.

[10] W.-J. Zhou, H. Tang, and J.-X. Chen, “Novel microfluidically tunable differential dual-mode patch filter,” *IEEE Microw. Wireless Compon. Lett.*, vol. 27, no. 5, pp. 461–463, May 2017.

[11] A. P. Saghati, J. S. Batra, J. Kameoka, and K. Entesari, “A miniaturized microfluidically reconfigurable coplanar waveguide bandpass filter with maximum power handling of 10 watts,” *IEEE Trans. Microw. Theory Techn.*, vol. 63, no. 8, pp. 2515–2525, Aug. 2015.

[12] S. N. McClung, S. Saeedi, and H. H. Sigmarsson, “Band-reconfigurable filter with liquid metal actuation,” *IEEE Trans. Microw. Theory Techn.*, vol. 66, no. 6, pp. 3073–3080, 2018.

[13] C. Arnold, J. Parlebas, and T. Zwick, “Reconfigurable waveguide filter with variable bandwidth and center frequency,” *IEEE Trans. Microw. Theory Techn.*, vol. 62, no. 8, pp. 1663–1670, Aug. 2014.

[14] S. Nam, B. Lee, B. Koh, C. Kwak, and J. Lee, “K-band fully reconfigurable pseudo-elliptic waveguide resonator filter with tunable positive and negative couplings,” *IEICE Trans. Commun.*, vol. 99, no. 10, pp. 2136–2145, Oct. 2016.

[15] B. Yassini, M. Yu, and B. Keats, “A *Ka*-band fully tunable cavity filter,” *IEEE Trans. Microw. Theory Techn.*, vol. 60, no. 12, pp. 4002–4012, Dec. 2012.

[16] B. Yassini, M. Yu, D. Smith, and S. Kellett, “A *Ku*-band high-*Q* tunable filter with stable tuning response,” *IEEE Trans. Microw. Theory Techn.*, vol. 57, no. 12, pp. 2948–2957, Dec. 2009.

[17] M. Yu, B. Yassini, B. Keats, and Y. Wang, “The sound the air makes: High-performance tunable filters based on air-cavity resonators,” *IEEE Microw. Mag.*, vol. 15, no. 5, pp. 83–93, Jul./Aug. 2014.

[18] S. Nam, B. Lee, C. Kwak, and J. Lee, “Contactless tuning plunger and its application to K-band frequency-tunable cavity filter,” *IEEE Trans. Microw. Theory Techn.*, vol. 67, no. 7, pp. 2713–2719, Jul. 2019.

[19] S.-W. Wong, F. Deng, J.-Y. Lin, Y.-W. Wu, L. Zhu, and Q.-X. Chu, “An independently four-channel cavity diplexer with 1.1-2.8 GHz tunable range,” *IEEE Microw. Wireless Compon. Lett.*, vol. 27, no. 8, pp. 709–711, Aug. 2017.

[20] S.-W. Wong *et al.*, “Independently frequency tunable dual- and triple-band filters in single cavity,” *IEEE Access*, vol. 5, pp. 11615–11625, Jul. 2017.

[21] D. Psychogiou and K. Sadasivan, “Tunable coaxial cavity resonator- based filters using actuated liquid metal posts,” *IEEE Microw. Wireless Compon. Lett.*, vol. 29, no. 12, pp. 763–766, Dec. 2019.

[22] N. Vahabisani, S. Khan, and M. Daneshmand, “Microfluidically reconfigurable rectangular waveguide filter using liquid metal posts,” *IEEE Microw. Wireless Compon. Lett.*, vol. 26, no. 10, pp. 801–803, Oct. 2016.

[23] D. Scarbrough, D. Psychogiou, D. Peroulii, and C. Goldsmith, “Low-loss, broadly-tunable cavity filter operating at UHF frequencies,” in *Proc. IEEE MTT-S Int. Microw. Symp. Dig.*, Jun. 2015, pp. 1–4.

Authorized licensed use limited to: SHENZHEN UNIVERSITY. Downloaded on December 12,2021 at 03:54:15 UTC from IEEE Xplore. Restrictions apply.

[24] M. S. Arif and D. Peroulis, "A 6 to 24 GHz continuously tunable, microfabricated, high-Q cavity resonator with electrostatic MEMS actuation," in *Proc. IEEE MTT-S Int. Microw. Symp. Tech. Dig.*, 2012, pp. 1–3.
[25] G. Chaudhary, Y. Jeong, and J. Lim, "Dual-band bandpass filter with independently tunable center frequencies and bandwidths," *IEEE Trans. Microw. Theory Techn.*, vol. 61, no. 1, pp. 107–116, Jan. 2013.
[26] E. J. Naglich, J. Lee, H. H. Sigmarsson, D. Peroulis, and W. J. Chappell, "Intersecting parallel-plate waveguide loaded cavities for dual-mode and dual-band filters," *IEEE Trans. Microw. Theory Techn.*, vol. 61, no. 5, pp. 1829–1838, May 2013.
[27] J. R. Chen, M. D. Benge, A. Anand, H. H. Sigmarsson, and X. Liu, "An evanescent-mode tunable dual-band filter with independently-controlled center frequencies," in *Proc. IEEE MTT-S Int. Microw. Symp. Tech. Dig.*, 2016, pp. 1–4.
[28] A. C. Guyette, "Intrinsically switched varactor-tuned filters and filter banks," *IEEE Trans. Microw. Theory Techn.*, vol. 60, no. 4, pp. 1044–1056, Apr. 2012.
[29] R. Gómez-García and A. C. Guyette, "Reconfigurable multi-band microwave filters," *IEEE Trans. Microw. Theory Techn.*, vol. 63, no. 4, pp. 1294–1307, Apr. 2015.
[30] J. S. Hong and M. J. Lancaster, *Microstrip Filters for RF/Microwave Applications*. New York, NY, USA: Wiley, 2001.

Rui-Sen Chen (Student Member, IEEE) was born in Fujian, China. He received the B.S. degree in electronics and information engineering from the Hunan University of Science and Technology, Hunan, China, in 2012, and the master's degree in electromagnetic field and radio technology from the South China University of Technology, Guangzhou, China, in 2015. He is currently working toward the doctor's degree with the College of Electronics and Information Engineering, Shenzhen University, Shenzhen, China.

He is a Research Assistant with the Faculty of Science and Technology, University of Macau, Macau from January to December 2020. His current research interests include microwave filter, antenna and cavity components.

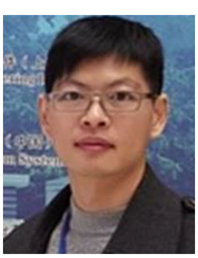

Sai-Wai Wong (Senior Member, IEEE) received the B.S. degree in electronic engineering from the Hong Kong University of Science and Technology, Hong Kong, in 2003, and the M.Sc. and Ph.D. degrees in communication engineering from Nanyang Technological University, Singapore, in 2006 and 2009, respectively.

From July 2003 to July 2005, he was an Electronic Engineer to lead the Electronic Engineering Department in China with two Hong Kong manufacturing companies. From May 2009 to October 2010, he was a Research Fellow with the ASTAR Institute for Infocomm Research, Singapore. Since 2010, he was an Associate Professor and later became a Full Professor with the School of Electronic and Information Engineering, South China University of Technology, Guangzhou, China. From July 2016 to September 2016, he was a Visiting Professor with the City University of Hong Kong, Hong Kong. Since 2017, he has been a Full Professor with the College of Electronics and Information Engineering, Shenzhen University, Shenzhen, China. So far, he has authored and coauthored more than 200 papers in international journals and conference proceedings. His current research interests include RF/microwave circuit and antenna design.

Dr. Wong was the recipient of the New Century Excellent Talents in University awarded by the Ministry of Education of China in 2013 and the Shenzhen Overseas High-Caliber Personnel Level C in 2018.

Jing-Yu Lin (Student Member, IEEE) received the B.E. degree in information security from Southwest Jiaotong University (SWJTU), Chengdu, China, in 2016, and the M.E. degree in electromagnetic fields and microwave technology from the School of Electronic and Information Engineering, South China University of Technology (SCUT), Guangzhou, China, in 2018. He is currently working toward the Ph.D. degree with the University of Technology Sydney (UTS), Ultimo, NSW, Australia.

From October 2017 to February 2019, he was as an exchange student with the University of Technology Sydney. His current research interests include microwave cavity circuit design.

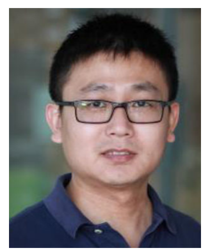

Yang Yang (Senior Member, IEEE) was born in Bayan Nur and grew up in Hohhot, Inner Mongolia, China. He received the Ph.D. degree in electronics engineering from ECSE in Clayton Campus, Monash University, Melbourne, VIC, Australia, in 2013.

He has three years industry experience with Rain Bird Australia, Deer Park, VIC serving as an Asia Pacific GSP Engineer, during 2012 and 2015. In April 2015, he returned to academia and served as a Senior Research Associate with the Centre for Collaboration in Electromagnetic and Antenna Engineering, Macquarie University, Macquarie Park, NSW, Australia. In April 2016, he was appointed as a Research Fellow with the State Key Laboratory of Terahertz and Millimeter Waves, City University of Hong Kong, Hong Kong. Since December 2016, he joined the University of Technology Sydney, Ultimo, NSW. He is currently a Senior Lecturer and a team leader of Millimetre-Wave Integrated Circuits and Antennas. He has more than 150 international peer reviewed publications in microwave and millimetre-wave circuits and antennas. His research interests include millimetre-wave and subterahertz technologies in 5G and biomedical applications.

Dr. Yang is currently an Associate Editor of IEEE ACCESS, and an Area Editor of *Microwave and Optical Technology Letters*. He is a current committee member of MTT-28 Biological Effects and Medical Applications. He is a recipient of the CST University Publication Award 2018, by CST, Dassault Systèmes and the corporate 2014 Global GSP Success Award (one globally).

Yin Li (Member, IEEE) received the B.S. degree in applied physics from the China University of Petroleum, Dongying, China, in 2009, the M.Eng. degree in electromagnetic field and microwave technology from the University of Electronic Science and Technology of China (UESTC), Chengdu, China, in 2012, and the Ph.D. degree in electrical and computer engineering with the University of Macau, Macau.

He is currently a Postdoctoral Fellow with the School of Electronics and Information from Shenzhen University, Shenzhen, China. From 2013 to 2015, he was a Research Assistant with the University of Hong Kong (HKU), Hong Kong. His current research interests include numerical modeling methods of passive microwave circuits, computational electromagnetics, and microwave circuits, frequency selectivity surface, and filtering antenna.

Authorized licensed use limited to: SHENZHEN UNIVERSITY. Downloaded on December 12,2021 at 03:54:15 UTC from IEEE Xplore. Restrictions apply.

Long Zhang (Member, IEEE) received the B.S. and M.S. degrees from the Huazhong University of Science and Technology (HUST), Wuhan, China, in 2009 and 2012, respectively, and the Ph.D. degree from the University of Kent, Canterbury, U.K, in 2017, all in electronic engineering.

He was a Research Fellow with the Poly-Grames Research Center, Polytechnique Montreal, Montreal, QC, Canada. He is currently an Assistant Professor with the College of Electronics and Information Engineering, Shenzhen University, Shenzhen, China. His current research interests include circularly polarized antennas and arrays, mm-wave antennas and arrays, tightly coupled arrays, reflectarrays and characteristics mode theory.

Dr. Zhang served as a Reviewer for several technique journals, including the IEEE TRANSACTIONS ON ANTENNAS AND PROPAGATION, the IEEE ANTENNAS AND WIRELESS PROPAGATION LETTERS, the *IET Microwaves, Antennas & Propagation*, and the *Electronic Letters*.

Yejun He (Senior Member, IEEE) received the Ph.D. degree in information and communication engineering from the Huazhong University of Science and Technology (HUST), Wuhan, China, in 2005.

He has been a Full Professor with the College of Electronics and Information Engineering, Shenzhen University, Shenzhen, China, where he is currently the Director of the Guangdong Engineering Research Center of Base Station Antennas and Propagation, and the Director of Shenzhen Key Laboratory of Antennas and Propagation, Shenzhen, China. He has authored or coauthored more than 180 research papers, books (chapters) and holds about 20 patents. His research interests include wireless communications, antennas, and radio frequency.

Dr. He was selected as a Pengcheng Scholar Distinguished Professor, Shenzhen, China. He was also a recipient of the Shenzhen Overseas High-Caliber Personnel Level B (“Peacock Plan Award” B) and Shenzhen High-Level Professional Talent (Local Leading Talent). He received the 2016 Shenzhen Science and Technology Progress Award and the 2017 Guangdong Provincial Science and Technology Progress Award. He served as General Chair of IEEE ComComAp 2019. He is a Fellow of IET, and the Chair of IEEE Antennas and Propagation Society-Shenzhen Chapter. He is serving as an Associate Editor of the IEEE NETWORK, the *International Journal of Communication Systems*, and *China Communications*.

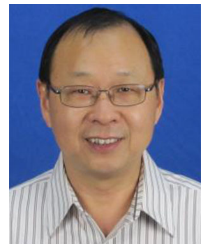

Lei Zhu (Fellow, IEEE) received the B.Eng. and M.Eng. degrees in radio engineering from the Nanjing Institute of Technology (now Southeast University), Nanjing, China, in 1985 and 1988, respectively, and the Ph.D. degree in electronic engineering from the University of Electro-Communications, Tokyo, Japan, in 1993.

From 1993 to 1996, he was a Research Engineer with Matsushita-Kotobuki Electronics Industries Ltd., Tokyo, Japan. From 1996 to 2000, he was a Research Fellow with the École Polytechnique de Montréal, Montréal, QC, Canada. From 2000 to 2013, he was an Associate Professor with the School of Electrical and Electronic Engineering, Nanyang Technological University, Singapore. He joined the Faculty of Science and Technology, University of Macau, Macau, as a Full Professor in August 2013, and has been a Distinguished Professor since December 2016. From August 2014 to August 2017, he served as the Head of the Department of Electrical and Computer Engineering, University of Macau. So far, he has authored or coauthored more than 580 papers in international journals and conference proceedings. His papers have been cited more than 10 000 times with the H-index of 51 (source: Scopus). His research interests include microwave circuits, planar antennas, periodic structures, and computational electromagnetics.

Dr. Zhu was the Associate Editors for the IEEE TRANSACTIONS ON MICROWAVE THEORY AND TECHNIQUES (2010–2013) and the IEEE MICROWAVE AND WIRELESS COMPONENTS LETTERS (2006–2012). He served as a General Chair of the 2008 IEEE MTT-S International Microwave Workshop Series on the Art of Miniaturizing RF and Microwave Passive Components, Chengdu, China, and a Technical Program Committee Co-Chair of the 2009 Asia–Pacific Microwave Conference, Singapore. He served as the member of IEEE MTT-S Fellow Evaluation Committee (2013–2015), and as the member of IEEE AP-S Fellows Committee (2015–2017). He was the recipient of the 1997 Asia–Pacific Microwave Prize Award, the 1996 Silver Award of Excellent Invention from Matsushita-Kotobuki Electronics Industries Ltd., and the 1993 First-Order Achievement Award in Science and Technology from the National Education Committee, China.

Authorized licensed use limited to: SHENZHEN UNIVERSITY. Downloaded on December 12,2021 at 03:54:15 UTC from IEEE Xplore. Restrictions apply.